IEEE Access
Multidisciplinary | Rapid Review | Open Access Journal

Received November 6, 2019, accepted November 17, 2019, date of publication November 21, 2019,
date of current version December 6, 2019.

Digital Object Identifier 10.1109/ACCESS.2019.2955027

Design and Implementation of a Novel Passive Magnetically Levitated Nutation Blood Pump for the Ventricular-Assist Device

GANG CHEN[1,2], LIGANG YAO[1], RONGYE ZHENG[1], LONG ZHANG[1], AND JIAXIN DING[1]
[1]School of Mechanical Engineering and Automation, Fuzhou University, Fuzhou 350116, China
[2]School of Mechanical and Electronic Engineering, Sanming University, Sanming 365004, China

Corresponding author: Ligang Yao (ylgyao@fzu.edu.cn)

This work was supported in part by the National Natural Science Foundation of China under Grant 51775114, and in part by the Natural Science Foundation of Fujian Province under Grant 2019J01822.

ABSTRACT Considering the wear in mechanical bearings and the requirement for sensors or electrical power in active magnetic bearings, a novel nutation blood pump using a passive magnetic spherical bearing was developed in this paper. A mathematical model was derived to calculate the magnetic forces of the bearing between two pairs of magnetic sleeves in the nutation process. The calculation results demonstrate that the fluctuations of magnetic forces enlarge with the increase in the nutation angle; the magnetic forces obviously increase with the decrease in the air gap, especially along the z-axis. The dynamic magnetic finite element simulation was carried out to validate the mathematical model. The simulation and calculation results of the magnetic forces show consistent trends and provide a theoretical basis for the parameter design. To validate the performance of the pump, computational fluid dynamics (CFD) analyses and in vitro experiments were conducted. The predicted values of the flow velocity vector through the pump, and the wall shear stress, demonstrate that the pump has an antithrombotic property and would not cause serious blood damage. The hydraulic experiment shows that a pressure rise can be achieved in the range of 60–140 mmHg, at a rotational speed of 600–1600 rpm and a flow rate of 0.4–6.7 L/min. The normalized index of hemolysis (NIH) of the nutation pump was 0.0043 ± 0.0008 g/100L. The in vitro tests indicate the feasibility of a magnetically levitated ventricular-assist nutation blood pump for further suspension stability and animal trials.

INDEX TERMS Nutation blood pump, passive magnetic levitation, bearing capacity, numerical simulation, ventricular assist device.

I. INTRODUCTION

Currently, because of some tricky problems in cardiac transplantation, such as implantation, the long-term management of transplant-related complications, and a serious lack of heart donors, one of the most effective measures for treating end-stage heart failure is the ventricular-assist device (VAD) [1], [2]. Most of the VADs in a clinical setting are designed as centrifugal blood pumps or axial flow blood pumps, such as HeartWare HVAD [3], HeartMate III [4], Terumo Dura-Heart [5], and Berlin Heart [6]. However, the advantages and disadvantages of centrifugal versus axial flow blood pumps are still in dispute. Mojtaba Koochaki et al. believe that a centrifugal blood pump with a large volume cannot conveniently be implanted in the body, and they proposed a new small axial blood pump [7]. Although the new axial flow design is much smaller than the centrifugal pump, it needs rotational speeds of 6000–6500 rpm to maintain an output flow rate of 0–11 L/min. However, a higher rotational speed may generate a higher magnitude of shear stress, which would result in hemolysis. Therefore, both the size and rotational speed reduction of the VAD for the total artificial heart (TAH) are important subjects. A miniature undulation pump was invented at the University of Tokyo, and various research projects have been carried out since 1992 [8]. However, because of the wear in the ball bearings and the malfunctions of the drive shaft and seal membranes, the durability of the undulation pump was not adequate [9]. Our research team proposed a novel miniscule ventricular assist nutation blood pump that realized a much smaller volume at the same flow

The associate editor coordinating the review of this manuscript and approving it for publication was Xiaodong Sun.

rate, compared with the undulation pump [10], [11]. A distinctive design characteristic of the nutation blood pump is that there are no seal membranes between the nutation disk and the pump housing, because the disk is supported by a spherical bearing located in the center of the pump cavity. The miniscule nutation blood pump has been proven to be feasible, but its mechanical bearing mechanism has potential problems at the contacting parts, which is suspected to be a cause of hemolysis and thrombogenicity.

The magnetically levitated pumps, as third-generation artificial heart pumps without a mechanical bearing that have high durability and lower hemolytic properties as well as antithrombogenicity, are leading candidates for the TAHs and VADs [12], [13]. Masuzawa *et al.* proposed a magnetically suspended blood pump with an axially levitated motor [14]. The axial force on the levitated impeller is balanced by the magnetic suspension system, and the axial position and tilting of the levitated impeller are controlled actively with the electromagnetic bearing. The WorldHeart company designed the Levacor VAD, which integrated a hybrid active and passive magnetic bearing to completely suspend a centrifugal impeller [15]. Although the rotor levitation can be achieved by active control with electromagnetic actuators, it requires electronics with an inherent vulnerability that can lead to the failure of sensors and signal leads. However, the passive magnetic bearings that do not need additional energy consumption and complex control systems are regarded as having the most potential as magnetic bearings for the support technology applied in blood pumps [16]. Wan *et al.* devised a permanent maglev impeller blood pump with a passive bearing, and demonstrated that the pump can achieve a dynamic balance by the external force of the blood flow [17]. Qian studied a permanent maglev rotator in a heart pump, which could be stabilized by using a non-permanent magnetic (PM) force acting together with a PM force [18]. Passive magnetic bearings achieve suspension by the magnetic force between the magnetic rings, and the calculation of the magnetic force is important. Ravaud *et al.* presented the analytical formulations of the magnetic field created by permanent-magnet rings, based on a Coulombian approach [19], [20]. Bachovchin *et al.* computed and analyzed the magnetic fields and magnetic forces from magnetic bearings made of circular Halbach permanent-magnet arrays [21]. Sun *et al.* presented a novel rotor structure with V-shaped permanents and an E-core stator for bearingless permanent magnet synchronous motors, and they analyzed the performance of control, torque and suspension force for the bearingless motors [22]–[25]. Xia presented a bionic artificial heart blood pump driven by permanent magnet and analyzed the magnetic field distribution and driving characteristics with a finite element method [26].

However, there is no research focusing on the magnetic forces from passive magnetic bearings in the nutation process. In addition, an oversimplified model is not suitable for describing the magnetic forces of the unique nutation characteristics. Above all, it is necessary to study the magnetically levitated nutation pump with a passive magnetic bearing and its service behavior.

II. METHODOLOGY

To conduct the study, a theoretical analysis, numerical simulation and in vitro test were applied. The theory of equivalent magnetic charges was applied to design the magnetically levitated spherical bearing. The numerical simulation was used not only to verify the mathematical model of magnetic levitation but also to predict the flow pattern and to calculate the pump performance. To validate the feasibility of the self-designed nutation blood pump and check the hemolysis performance, in vitro experiments were performed.

A. STRUCTURE AND MECHANISM

The current magnetically levitated nutation pump is based on the previous mechanical contact spherical bearing nutation pump that was designed by our laboratory. To reduce the mechanical friction and wear, a new structure for the passive magnetic spherical bearing was designed. Here, the inclined sleeve driven directly by the motor shaft to generate the nutation motion has been eliminated, and the nutation disk is driven by a pair of permanent magnets outside the pump chamber. As shown in Figure 1(a), two permanent magnets are arranged diagonally in the rotary sleeve and seven permanent magnets are uniformly installed in the edge of the nutation disk. These magnets in the nutation disk are attracted by the two magnets in the sleeve. The attraction between the magnets keeps the nutation disk tilted and in contact with the inner cones of the upper and lower covers in the lines. The rotary sleeve is driven by a miniature brushless DC motor, and the nutation disk swings up and down with the rotation of the sleeve. The internal vessel of the pump is surrounded by part of a sphere and is inside two inner cones of the upper and lower covers. Considering the compartment that lies below the nutation disk, the lower compartment is divided into two areas by the contact lines. When the contact lines move counterclockwise with the nutation disk, the inlet area increases, continuously generating negative pressure that causes the fluid to flow into it. At the same time, the outlet area diminishes, the fluid is pushed through the outlet, and the pump mechanism activated. Figure 1(b) shows the motion of the nutation disk and the orientation of the fluid flow.

The nutation disk is supported by a spherical magnetic bearing that is located in the spherical cavity between the upper and lower covers and is nutated together with the nutation disk. As a result of the technical difficulties in the processing and magnetization of the spherical permanent magnets, it is difficult to implement the magnetic suspension of the spherical bearing directly using spherical permanent magnets with homogeneous magnetization [27]. Therefore, the permanent magnets of the spherical bearing are designed as magnetic fan-shaped sleeves that are inserted into the spherical pairs of the nutation disk and the spherical cavities of the upper and lower covers. To make the nutation disk swing up and down with no self-rotation, a pin shaft is

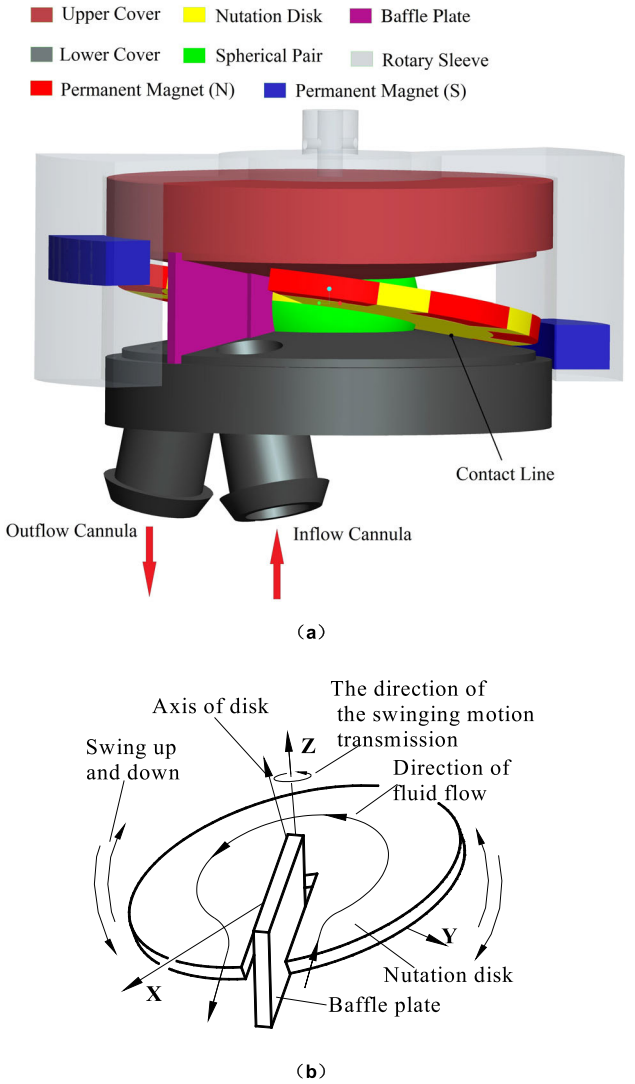

FIGURE 1. (a) Schematic diagram of the magnetically levitated nutation pump model. (b) The motion of the nutation disk and the orientation of fluid flow.

designed in the middle of the opening of the nutation disk and is confined to move only in the groove of the baffle plate. Thus, the magnetic fan-shaped sleeves in the spherical bearing always keep nutating, only with no self-rotating when the pump works. The suspension of the spherical bearing is achieved by the repulsive force between the magnetic fan-shaped sleeves in the spherical pairs and covers. The schematic diagram of the pump is shown in Figure 1, and the dimensions of the pump are given in Table 1.

B. MATHEMATICAL MODEL

In the working process of the pump, the fan-shaped magnetic sleeves in the covers are stationary, but the axes of the fan-shaped magnetic sleeves in the spherical pair are changing continuously with the swing of the nutation disk. Therefore, the axes between the paired fan-shaped magnetic sleeves in the covers and spherical pair are tilted. To study the magnetic force and bearing capacity of the magnetically

TABLE 1. Pump dimensions.

Parameters	Dimensions
Assembly diameter	52 mm
Length of pump (Including 10 mm for inlet and outlet cannula from each size)	30.4 mm
Inner sphere diameter of pump shell	38.1 mm
Diameter of nutation disk	38 mm
Nutation disk thickness	2 mm
Diameter of spherical pair	16 mm
Conical degree of upper (lower) cover cone	10°
Outer diameter of magnets in spherical pair	12 mm
Inner diameter of magnets in spherical pair	8 mm
Outer diameter of magnets in upper and lower covers	20.4 mm
Inner diameter of magnets in upper and lower covers	16.4 mm

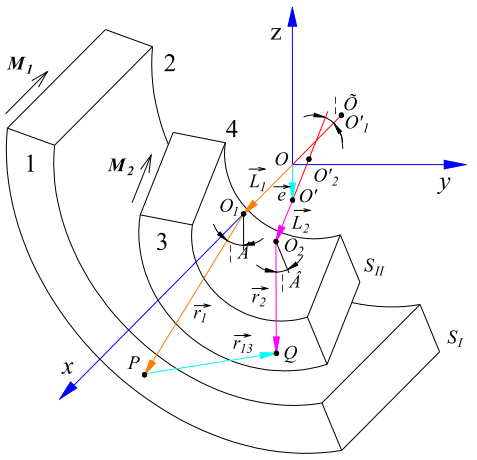

FIGURE 2. The relative position of the paired permanent magnets in a spherical bearing.

levitated spherical bearing, a pair of fan-shaped magnetic sleeves is used for the study, and the physical model is shown in Figure 2. The two fan-shaped sleeves (S_I and S_{II}) are made of a neodymium iron boron (NdFeB) permanent magnet, with dimensions R_1, R_2, and $2L_1$, and R_3, R_4, and $2L_2$, respectively (as shown diagrammatically in Figure 2). The sleeve lengths are equal (i.e., $L_1 = L_2$), and they are magnetized along their axial direction. The magnetic charge densities on the end of the surfaces of the sleeve are σ_1 and σ_2, which are supposed to be rigid and uniform.

The sleeves in the spherical pair are designed as an eccentric structure. S_I is fixed in the pump cover, and S_{II} in the spherical pair has an eccentricity with e along the OO' direction. $O_1O'_1$ and $O_2O'_2$ are the axes of S_I and S_{II} with the centers of O and O', respectively. S_{II} rotates φ degrees around its center in the plane xoz because the nutation disk is only a nutation without rotation. The variable angle, φ, depends on the nutation angle, θ, and it swings between $-\theta$ and θ.

As surfaces 1 and 2 have the same geometry, the integration variables in surface 2 can be expressed by the variables in surface 1 ($\boldsymbol{r_1}$,α). Similarly, the integration variables in surface 4 can be expressed by the variables in surface 3 ($\boldsymbol{r_2}$, β). Variable α is the direction angle of vector $\boldsymbol{r_1}$ in surface1, and

β is the direction angle of vector $\boldsymbol{r_2}$ in surface 3. From the theory of equivalent magnetic charges, the interaction force between the charges on some of the microsurface areas, P, in surface 1, and those on some of the other microsurface areas, Q, in surface 3, is [28]–[31]:

$$d\vec{F}_{mn} = \frac{\sigma_1\sigma_2}{4\pi\mu_0} \cdot \frac{r_1 r_2 dr_1 dr_2 d\alpha d\beta}{|\vec{r}_{mn}|^3} \cdot \vec{r}_{mn} \tag{1}$$

where $m = 1, 2$; n $= 3, 4$; and μ_0 is the permeability of the vacuum, $\mu_0 = 4\pi \times 10^{-7}$ H·m−1.

From the magnetic relation [32], the face densities of the magnetic charges of the rare earth permanent magnets can be expressed as follows:

$$\sigma_1 = B_{r1}, \quad \sigma_2 = B_{r2} \tag{2}$$

where B_{r1} and B_{r2} are the remanences of the magnetic sleeves.

In this case, we will assume, without a loss of generality, that the attractive force is positive and the repulsion is negative. Therefore, the differential form of the total interaction force between S_{II} in the spherical pair and S_I in the pump cover is as follows:

$$d\vec{F} = -d\vec{F}_{13} + d\vec{F}_{23} + d\vec{F}_{14} - d\vec{F}_{24} \tag{3}$$

which can be written in projective form along the coordinate axes as follows:

$$\begin{cases} d\vec{F}_x = -d\vec{F}_{13x} + d\vec{F}_{23x} + d\vec{F}_{14x} - d\vec{F}_{24x} \\ d\vec{F}_y = -d\vec{F}_{13y} + d\vec{F}_{23y} + d\vec{F}_{14y} - d\vec{F}_{24y} \\ d\vec{F}_z = -d\vec{F}_{13z} + d\vec{F}_{23z} + d\vec{F}_{14z} - d\vec{F}_{24z} \end{cases} \tag{4}$$

and combining Equations (1) and (3), the integrative form of the total force is as follows:

$$\begin{cases} F_x = \dfrac{\sigma_1\sigma_2}{4\pi\mu_0} \int_0^{2\pi}\int_0^{2\pi}\int_{R_1}^{R_2}\int_{R_3}^{R_4} \left(-\dfrac{r_{13x}}{|r_{13}|^3} + \dfrac{r_{23x}}{|r_{23}|^3} + \dfrac{r_{14x}}{|r_{14}|^3} - \dfrac{r_{24x}}{|r_{24}|^3}\right) \\ \times r_1 r_2 dr_1 dr_2 d\alpha d\beta \\ F_y = \dfrac{\sigma_1\sigma_2}{4\pi\mu_0} \int_0^{2\pi}\int_0^{2\pi}\int_{R_1}^{R_2}\int_{R_3}^{R_4} \left(-\dfrac{r_{13y}}{|r_{13}|^3} + \dfrac{r_{23y}}{|r_{23}|^3} + \dfrac{r_{14y}}{|r_{14}|^3} - \dfrac{r_{24y}}{|r_{24}|^3}\right) \\ \times r_1 r_2 dr_1 dr_2 d\alpha d\beta \\ F_z = \dfrac{\sigma_1\sigma_2}{4\pi\mu_0} \int_0^{2\pi}\int_0^{2\pi}\int_{R_1}^{R_2}\int_{R_3}^{R_4} \left(-\dfrac{r_{13z}}{|r_{13}|^3} + \dfrac{r_{23z}}{|r_{23}|^3} + \dfrac{r_{14z}}{|r_{14}|^3} - \dfrac{r_{24z}}{|r_{24}|^3}\right) \\ \times r_1 r_2 dr_1 dr_2 d\alpha d\beta \end{cases} \tag{5}$$

The coordinate system of S_I is the static coordinate system, $o_0 - x_0y_0z_0$, and the origin of the static coordinate system is located at the center of the nutation disk spherical pair. The coordinate system of S_{II} is a dynamic coordinate system, $o_1 - x_1y_1z_1$, and the origin of the dynamic coordinate system offsets e along the $-z_0$ direction. The position of $o_1 - x_1y_1z_1$ relative to $o_0 - x_0y_0z_0$ can be described as follows: (i) S_{II} has eccentricity e along the $-z_0$ direction, and rotates θ degrees around the y_1 axis, which is the initial position shown in Figure 3a; (ii) S_{II} rotates θ_x degrees around the x_1 axis, and

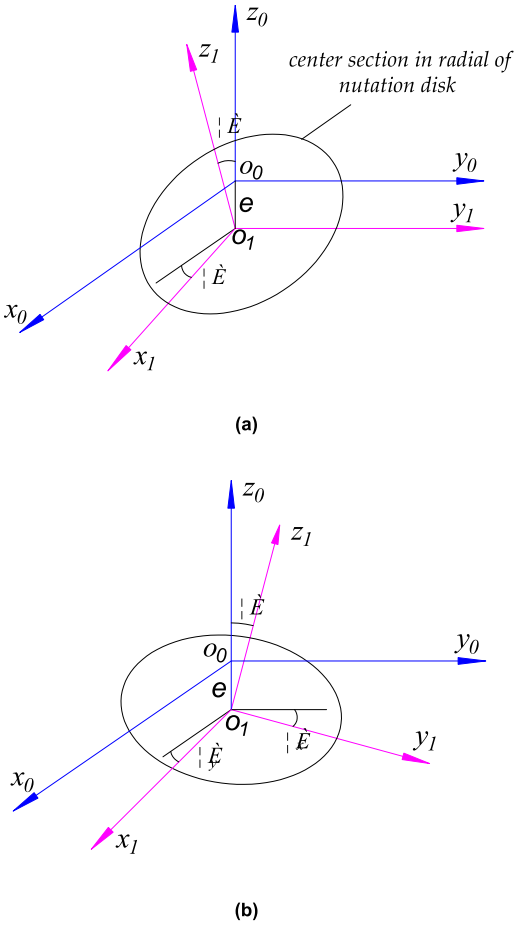

FIGURE 3. The transformation steps of the dynamic coordinate system, namely: (a) the initial position. (b) the arbitrary position.

the angle between the x_1 and x_0 axis becomes θ_y, which is the arbitrary position shown in Figure 3b.

Angles θ_x and θ_y vary periodically, and their relationship over time is as follows:

$$\begin{cases} \theta_x = -\dfrac{4\theta}{T}t \left(0 \le t < \dfrac{T}{4}\right) \\ \theta_x = \dfrac{4\theta}{T}t - 2\theta \left(\dfrac{T}{4} \le t < \dfrac{3T}{4}\right) \\ \theta_x = -\dfrac{4\theta}{T}t + 4\theta \left(\dfrac{3T}{4} \le t \le T\right) \\ \theta_y = \dfrac{4\theta}{T}t - \theta \left(0 \le t < \dfrac{T}{2}\right) \\ \theta_y = -\dfrac{4\theta}{T}t + 3\theta \left(\dfrac{T}{2} \le t \le T\right) \end{cases} \tag{6}$$

where θ is the nutation angle and T is the rotation period.

The composition of vector $\vec{r}_{13}$ in Equation (5) can be determined from Figure 2 and is shown in Figure 4. The projections of the vectors in Figure 4 on the coordinate axes are given in Table 2. Hence, the components of $\vec{r}_{13}$ along the coordinate axes and the magnitude $|\vec{r}_{13}|$ are

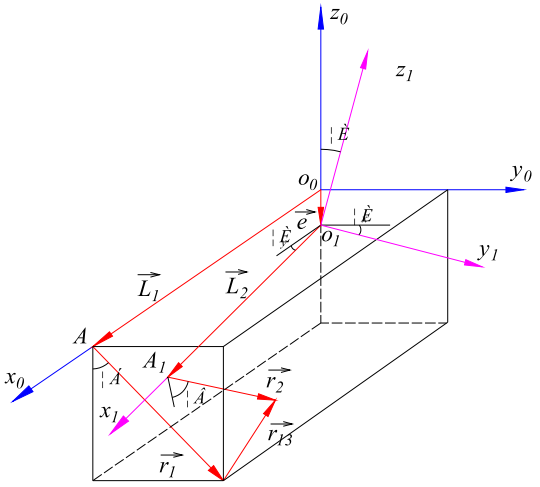

FIGURE 4. Composition of vector $\vec{r}_{13}$.

TABLE 2. Projections of the vectors from equation (7).

Vector	Projection on x axis	Projection on y axis	Projection on z axis
$\boldsymbol{e}$	0	0	$-e$
$\boldsymbol{L_1}$	L_1	0	0
$\boldsymbol{L_2}$	$L_2 cos\theta_{ym}$	0	$-L_2 sin\theta_{ym}$
$\boldsymbol{r_1}$	0	$r_1 sin\alpha$	$r_1 cos\alpha$
$\boldsymbol{r_2}$	$-r_2 cos\beta sin\theta_{ym} cos\theta_{xm}$	$r_2 sin\beta cos\theta_{xm}$	$-r_2 cos\beta cos\theta_{xm} cos\theta_{ym}$

as follows:

$$\begin{cases} \vec{r}_{13} = -\vec{L}_1 - \vec{r}_1 + \vec{L}_2 + \vec{r}_2 + \vec{e} \\ \vec{r}_{13x} = \vec{r}_{13}.\vec{i} = -L_1 + L_2\cos\theta_y - r_2\cos\beta\sin\theta_y\cos\theta_x \\ \vec{r}_{13y} = \vec{r}_{13}.\vec{j} = -r_1\sin\alpha + r_2\sin\beta\cos\theta_x \\ \vec{r}_{13z} = \vec{r}_{13}.\vec{k} = -e - L_2\sin\theta_y + r_1\cos\alpha \\ -\,r_2\cos\beta\cos\theta_y\cos\theta_x \\ |\vec{r}_{13}| = \sqrt{r_{13x}^2 + r_{13y}^2 + r_{13z}^2} \end{cases} \tag{7}$$

where $\vec{i}$, $\vec{j}$, and $\vec{k}$ are the unit vectors along the coordinate directions.

Similarly, $\vec{r}_{14}$, $\vec{r}_{23}$, and $\vec{r}_{24}$ can be expanded as follows:

$$\begin{cases} \vec{r}_{14} = -\vec{L}_1 - \vec{r}_1 - \vec{L}_2 + \vec{r}_2 + \vec{e} \\ \vec{r}_{14x} = \vec{r}_{14}.\vec{i} = -L_1 - L_2\cos\theta_y - r_2\cos\beta\sin\theta_y\cos\theta_x \\ \vec{r}_{14y} = \vec{r}_{14}.\vec{j} = -r_1\sin\alpha + r_2\sin\beta\cos\theta_x \\ \vec{r}_{14z} = \vec{r}_{14}.\vec{k} = -e + L_2\sin\theta_y + r_1\cos\alpha \\ -\,r_2\cos\beta\cos\theta_y\cos\theta_x \\ |\vec{r}_{14}| = \sqrt{r_{14x}^2 + r_{14y}^2 + r_{14z}^2} \end{cases} \tag{8}$$

$$\begin{cases} \vec{r}_{23} = \vec{L}_1 - \vec{r}_1 + \vec{L}_2 + \vec{r}_2 + \vec{e} \\ \vec{r}_{23x} = \vec{r}_{23}.\vec{i} = L_1 + L_2\cos\theta_y - r_2\cos\beta\sin\theta_y\cos\theta_x \\ \vec{r}_{23y} = \vec{r}_{23}.\vec{j} = -r_1\sin\alpha + r_2\sin\beta\cos\theta_x \\ \vec{r}_{23z} = \vec{r}_{23}.\vec{k} = -e - L_2\sin\theta_y + r_1\cos\alpha \\ -\,r_2\cos\beta\cos\theta_y\cos\theta_x \\ |\vec{r}_{23}| = \sqrt{r_{23x}^2 + r_{23y}^2 + r_{23z}^2} \end{cases} \tag{9}$$

TABLE 3. Material parameters and dimensions of the magnets.

Material parameters	Dimensions
	Sleeve S_I
Remanence	Length $2L_1$ = 4mm
B_r = 1T	Inner radius R_1 = 8.2 mm
Coercive force	Outer radius R_2 = 10.2 mm
H_c = 955 kA.m	Sleeves S_{II}
Energy product	Length $2L_2$ = 4 mm
$(BH)_{max}$= 223 kJ.m^{-3}	Inner radius R_3 = 4 mm
	Outer radiusR_4 = 6 mm

and

$$\begin{cases} \vec{r}_{24} = \vec{L}_1 - \vec{r}_1 - \vec{L}_2 + \vec{r}_2 + \vec{e} \\ \vec{r}_{24x} = \vec{r}_{24}.\vec{i} = L_1 - L_2\cos\theta_y - r_2\cos\beta\sin\theta_y\cos\theta_x \\ \vec{r}_{24y} = \vec{r}_{24}.\vec{j} = -r_1\sin\alpha + r_2\sin\beta\cos\theta_x \\ \vec{r}_{24z} = \vec{r}_{24}.\vec{k} = -e + L_2\sin\theta_y + r_1\cos\alpha \\ -\,r_2\cos\beta\cos\theta_y\cos\theta_x \\ |\vec{r}_{24}| = \sqrt{r_{24x}^2 + r_{24y}^2 + r_{24z}^2} \end{cases} \tag{10}$$

By substituting Equation (2) and Equations (6)–(10) into Equation (5), the components of the total interaction force can be calculated.

C. SIMULATION

The 3D magnetic simulation analyses were carried out to calculate the magnetic force of the proposed magnetic levitation structure, and to verify the mathematical model. The magnetic field distribution of the magnetic bearing was investigated with the physics mode of rotating machinery and magnetic, which provide a scientific basis for the design of the pump. To realize the disk magnetically levitating, the magnets simulated in the spherical bearing were neodymium magnets. Table 3 presents the material parameters and dimensions of the magnets.

The characteristics of the internal flow field of the pump are complex, and the flow conditions in the nutation blood pump are considered turbulent. To validate the flow velocity in the pump and the distribution shear stress, the *RNG k-ε* turbulence model was used to solve the flow domain with ANSYS Fluent, using the user-defined functions. The blood was treated as an incompressible Newtonian fluid, with a density of 1060 kg/m^3 and viscosity of 0.0036 kg/m·s [33]. The pressures were selected as the inflow and outflow conditions, and no-slip was selected as the wall boundary condition. The differential pressure of the inlet and outlet was 100 mmHg. The mesh model consisted of 164591 tetrahedron elements and 29114 mesh nodes. The discretization of the governing equations was performed using a second order type, and the residual target was set before the time, for the sake of accuracy.

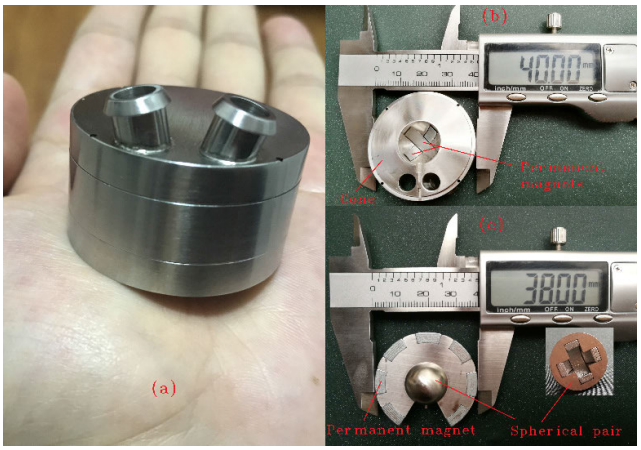

FIGURE 5. (a) Prototype pump. (b) Image of the lower cover. (c) Image of the nutation disk.

D. MANUFACTURING AND EXPERIMENTATION

The CAD model of the pump was established and all the parts were manufactured using biocompatible stainless steel 316LS, except for the rotary sleeve, which was made with a resin material. Each part was then polished using diamond paste to achieve a mirror-like surface, as shown in Figure 5. To drive the nutation disk into a swing motion, seven fan-shaped N45 grade neodymium iron boron (NdFeB) permanent magnets, with an outer diameter of 38 mm, an inner diameter of 30 mm, and a thickness of 2 mm, were implanted into the edge of the nutation disk. To facilitate the installation of the magnetic sleeves, the magnetic sleeves were processed into a fan-shape and then assembled in the covers and a spherical pair. The eccentricity of the magnetic sleeves in the spherical bearing was 1.2 mm, and the nutation angle of the pump was 10°. To avoid the nutation disk being rotated in contact with the pump housing and to minimize the clearance flow, the gap length in the radial direction between the disk and the inner housing was approximately 0.08 mm.

The in vitro experiments were performed to confirm the principle of the self-designed pump and check the hemolysis performance. The test platform of the self-designed pump was built in accordance with the ASTM F1841 standard test procedure, from the American Society for Testing and Materials (ASTM) [34], as shown in Figure 6. The flow pressure curve of the pump was tested with fresh porcine blood as a fluid, by adjusting the speed and after-load of the pump. The in vitro simulated circulation system was composed of a blood storage bag (with sodium citrate as the anticoagulant), silicone hose, pressure regulating valve, flowmeter, differential pressure gauge, motor, and power supply system. The preload of the pump was adjusted according to the height of the storage bag and the after-load was regulated by the pressure regulating valve. At each pressure load, the motor speed was gradually adjusted, and the output flow rate of the pump was recorded at each speed after the flow became stable. The temperature of the VAD system was monitored by an infrared thermometer placed close to the pump, motor, and

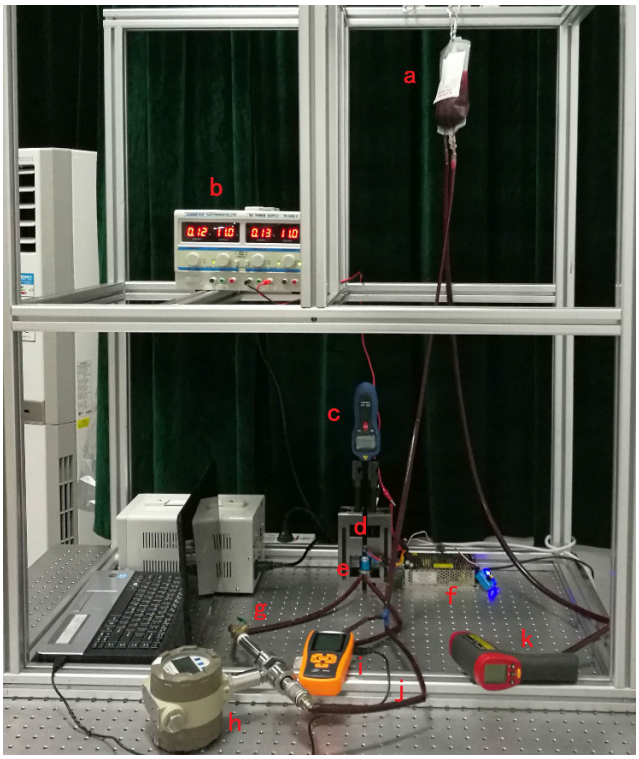

FIGURE 6. The test platform for in-vitro experiments: (a) Blood storage bag. (b) Power supply system. (c) Infrared velocimeter. (d) Motor. (e) Pump. (f) Control device. (g) Throttle valve. (h) Flowmeter. (i) Differential pressure gauge. (j) Silicone hose. (k) Infrared thermometer.

pipe wall, to accurately measure the operating temperature. To reduce the influence of air bubbles on hemolysis results, the fresh porcine blood for the hemolysis test was stored at 2-5°C for 2 days. The hemolysis tests with 500 mL were carried out three times under the conditions where the head of the pump was 100 mmHg with a flow of 5 L/min. Plasma free hemoglobin and hematocrit were measured with 5 mL blood samples collected at 30-min intervals. The experimental NIH level was calculated using the following formula [35]:

$$NIH_{\exp}[g/100L] = \Delta FHb \times (100 - H_t) \times \frac{Vol}{Q \times \Delta t} \quad (11)$$

where ΔFHB is the increase in plasma free hemoglobin (g/L), Vol is the total blood volume (m^3), H_t is the hematocrit (%), Q is the blood flow (L/min), and Δt is the sampling time (min).

III. RESULTS

A. NUMERICAL RESULTS

In the working process of the nutation pump, the relative position between magnets S_I and S_{II} in the spherical bearing, and hence the magnetic field, is altered, and the interaction force changes with the magnetic field. With the calculation of the mathematical model, comparisons between the forces for the different states of magnets in the spherical bearing in one nutation period are shown in Figure 7. The air gap, g, and nutation angle, θ, both have a significant influence on F_x,

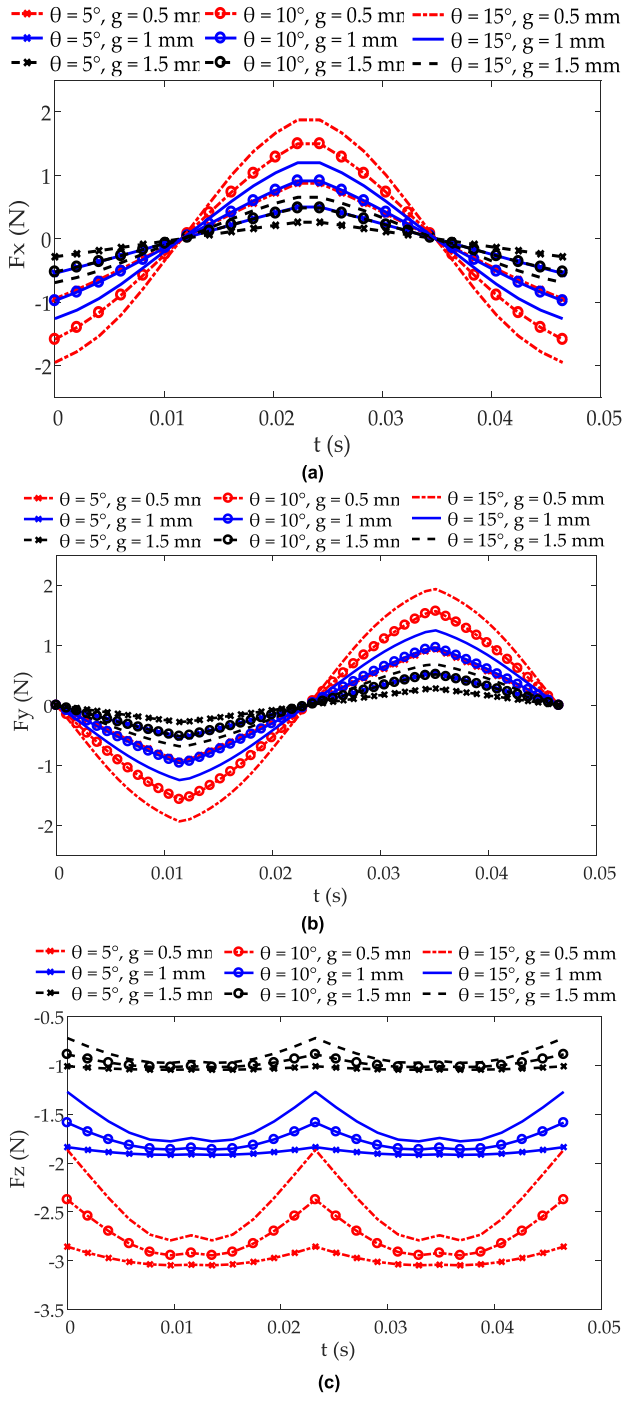

FIGURE 7. Force comparison under different air gaps and nutation angles.

F_y, and F_z. The magnetic forces increase with the increase of eccentricity (the decrease in the air gap) when the nutation angle is fixed, especially F_z, and the variation range of the magnetic forces obviously increases with the increase in the nutation angle. For example, when the nutation angle is $\theta = 10°$ and the air gap is $g = 0.5$ mm, the maximum is $F_z \approx -2.3750$ N, and when $\theta = 10°$ and $g = 1.5$ mm, the maximum is $F_z \approx -0.8875$N. When $g = 0.5$ mm and $\theta = 15$, the maximum difference is $|\Delta F_z| = 0.9270$ N; even when $g = 0.5$ mm and $\theta = 5°$, the maximum difference of $|\Delta F_z|$ is only approximately 0.1910 N. Fx and Fy are the radial magnetic forces that fluctuate around 0 when the nutation angle is small. F_z is the axial magnetic force that depends on the air gap. The nutation disk maintains noncontact with the inner wall of the pump because the radial movement of the disk is restricted by the flat clapboard. Therefore, it is anticipated that the radial magnetic force will be small when the axial magnetic force is large enough. As expected, the adequate suspension axial magnetic force F_z can be obtained by the appropriate design of the eccentricity. The magnetic force can be considered constant when the nutation angle is very small, which is conducive to the magnetic suspension stability.

B. SIMULATION RESULTS

To verify the mathematical model of the interaction force, the dynamic magnetic finite element analysis simulation was carried out. Figure 8a and 8b demonstrates the magnetic flux density of the magnets in a spherical bearing at a certain moment. There is a constant changing interactive force between the magnets in the covers and spherical pairs, as the spherical pair is nutating with the nutation disk swinging up and down. Figure 9c shows a comparison of the simulated and numerical results of the magnetic forces along the z-axis when θ is 10° and for different air gaps. The maximum difference of ΔF_z of the simulated and numerical results is 0.206 N and 0.215 N, respectively, when the gap is 1 mm. The maximum deviation between the simulated and numerical results is approximately 4.2% when the gap is 1 mm, which indicates that the numerical data are consistent with the simulations, showing the general validity of Equation (5).

Figure 9a shows the velocity vectors at 1450 rpm and a 5 L/min flow rate throughout the pump. The fluid enters from the left side into the pump chamber, along with the motion of the nutation disk. As expected, the flow velocity in the pump is uniform, except that the inlet and outlet are higher because of the small cross-section, and the maximum flow velocity is approximately 4.5 m/s. The trend in the direction of the flow field inside the pump is consistent with the flow from the inlet to the outlet and there is no recirculation region and flow dead zone in the internal flow field, verifying that the nutation pump has an antithrombotic property.

The hemolysis performance of the blood pump can be studied through the analysis of the shear stress, because it has been proven that the essential reason for hemolysis is caused by shear stress [36], [37]. The wall shear stress has been analyzed, as shown in Figure 9b, at a 1450 rpm rotational speed and 100 mmHg pressure head. Figure 9c shows the stress histogram of the elements. More than 89% of the particles have a scalar stress less than 200 Pa. The regions where these high shear stress elements occur are at the contact lines between the nutation disk and the pump covers. Blood passing through this region is more prone to hemolysis. However, the maximum shear stress is approximately 700 Pa, and its exposure time is within 0.0414 s. According to the literature reports, these shear stress and exposure time

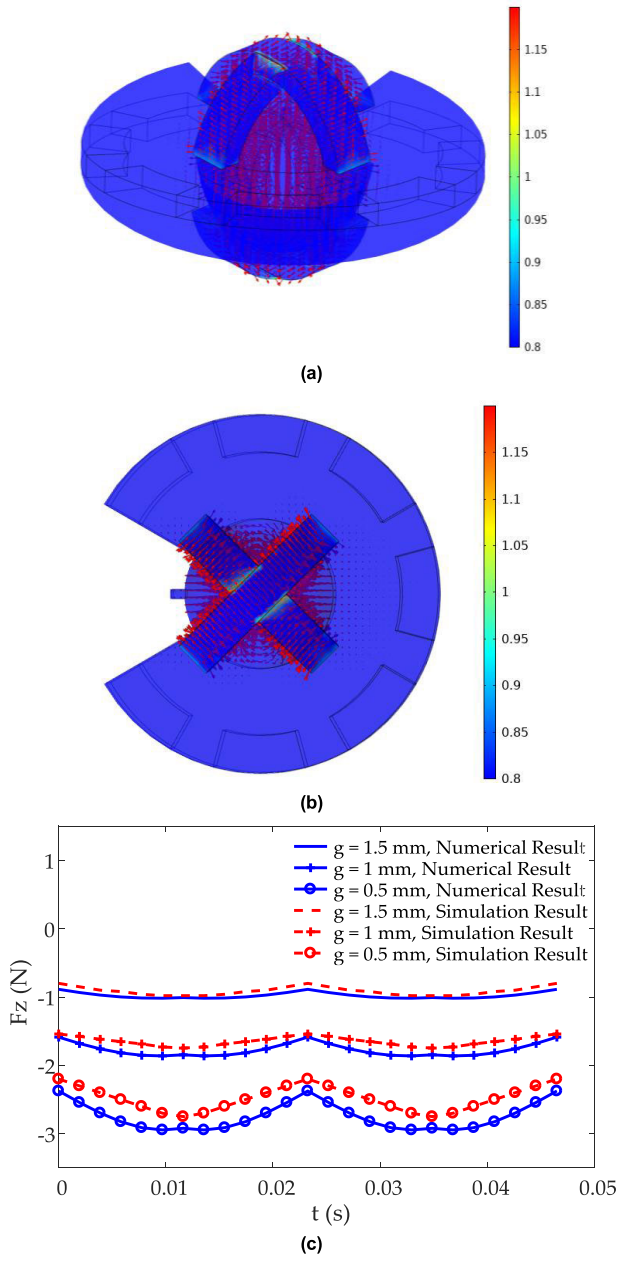

FIGURE 8. Magnetic simulation results, namely: (a) magnetic flux density for magnets in a spherical bearing; (b) magnetic flux density in an xy cross plane; (c) magnetic forces comparison of simulated and numerical results.

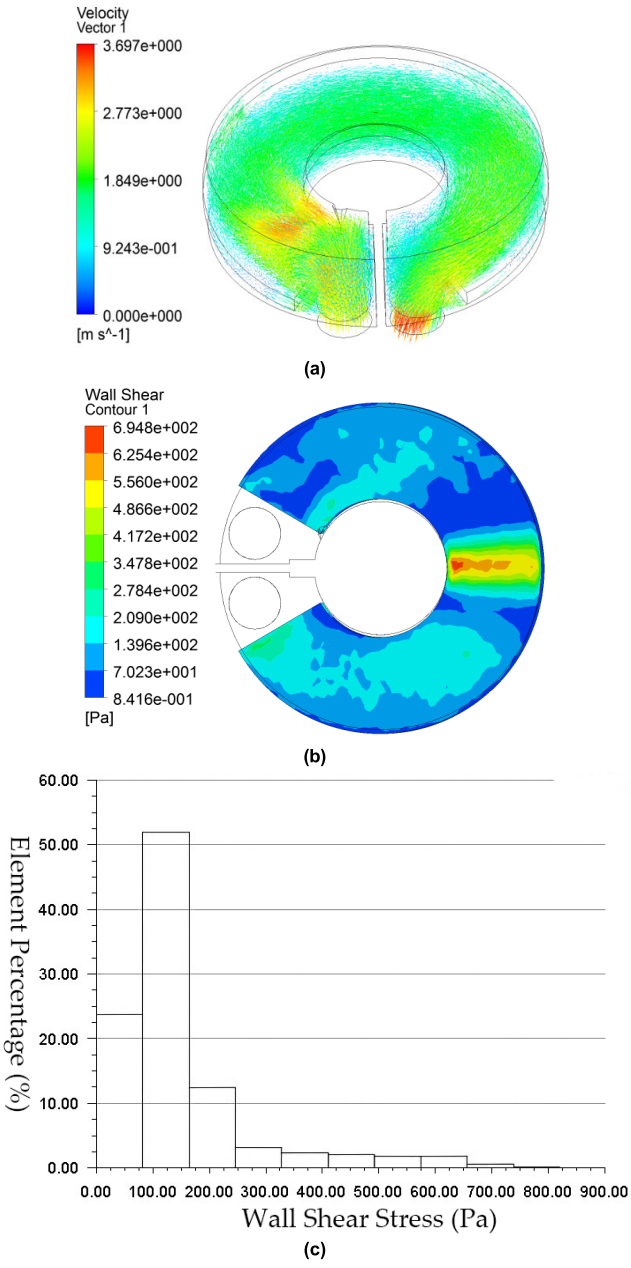

FIGURE 9. CFD performance simulation results: (a) velocity vectors of the pump at 1450 rpm and 5 L/min; (b) the wall shear stress along the pump at 1450 rpm rotational speed and 100 mmHg pressure; (c) shear stress histogram showing percentage distribution of stress in an element with increments of 100 Pa.

measurements would not cause any serious damage to the red blood cells [38], [39]. Hence, our designed pump works in a completely safe domain.

C. EXPERIMENTAL RESULTS

The measured value at each measurement point has been plotted into the curve shown in Figure 10a, which shows the hydraulic performance of the self-designed magnetic levitation pump system, with fresh porcine blood as the fluid in a mock circulation. More than 5 L/min of continuous output could be obtained against 100 mmHg of pressure load. When the head of the pump is 100 mmHg with a flow of 5 L/min, the rotational speed is approximately 1450 rpm. In addition, the pressure difference between the inlet and outlet rose from 80 to 100 mmHg, and the output flow rate decreased only approximately 0.6 L/min when the motor speed was 1400 rpm. The test results suggest that the output flow of this pump is stable at a different pressure. Moreover, there was no obvious rise in the temperature of the VAD system during the experiment. The temperature variation of the motor shell was between 34.0 °C and 35.3 °C when the system performed steadily.

The results of the in vitro hemolysis test repeated three times are shown in Table 4. The experimental NIH of the

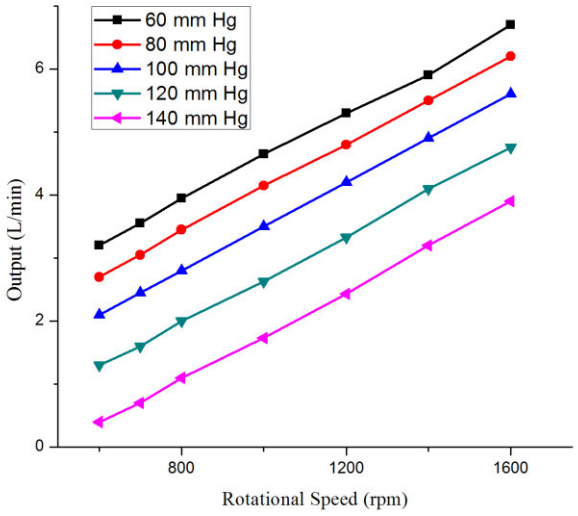

(a)

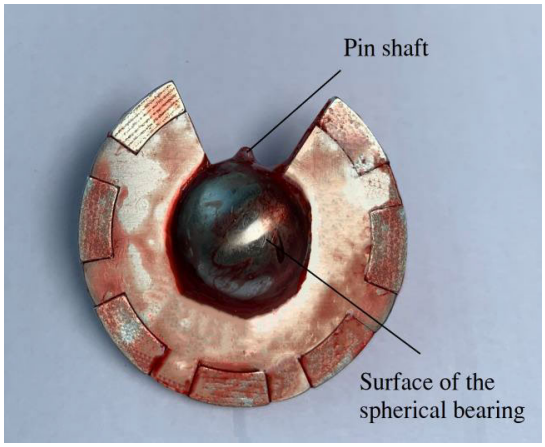

(b)

FIGURE 10. The experimental results are as follows: (a) hydraulic performance of the pump; (b) the nutation disk after the blood test.

TABLE 4. The results of in vitro hemolysis test (n = 18).

Group	H_t	NIH (g/100L)					
		0.5 h	1 h	1.5 h	2 h	2.5 h	3 h
1	34.2	0.0035	0.0039	0.0044	0.0043	0.0051	0.0056
2	33.6	0.0037	0.0032	0.0041	0.0046	0.0052	0.0054
3	33.4	0.0031	0.0034	0.0036	0.0042	0.0049	0.0052

nutation pump was calculated as 0.0043 ± 0.0008 g/100L, which shows that the pump would not cause serious blood damage; these results are consistent with the CFD result. Figure 10b shows the disassembled nutation disk after a blood test. Upon close examination, it was observed that there is no obvious wear on the surface of the spherical bearing and the pin shaft of the nutation disk. However, there is some blood that accumulates near the contact region between the spherical bearing and nutation disk, which can cause thrombosis in long-term use. The accumulated blood showed that the possible area of backflow was a result of the air gap in the magnetic spherical bearing. Although the magnetic levitation spherical bearing can eliminate friction and wear, the suspension air gap would cause a clearance backflow.

IV. CONCLUSION

In this paper, the principle of a passive magnetically levitated nutation pump was developed, confirmed by computer calculation, and demonstrated to work in a model. Focusing on the passive magnetic spherical bearing, a mathematical model was derived to calculate the interaction forces between the magnetic sleeves in the nutation process, using the equivalent magnetic charges theory. Through the in vitro blood test, the feasibility of the theoretical model of the pump was validated. The conclusions of this paper are as follows.

1. The bearing capacity of the spherical bearing increases with the increase in eccentricity. The fluctuation of the magnetic force is obviously affected by the nutation angle. When the eccentricity is fixed and the nutation angle is very small, the fluctuation of the magnetic force is very little.

2. The dynamic magnetic finite element analysis results are in good agreement with the numerical results, which verifies the mathematical model for the case where the magnetic sleeves in the spherical bearing were eccentric and nutating.

3. The CFD analysis of the blood flow velocity vector and wall shear in the pump revealed that this pump would not cause any serious blood damage, which shows good correlation with experimental data, validating the model.

4. The satisfactory hydraulic performance and low NIH values validated the design concept of the proposed magnetic levitated nutation pump. The study paves a foundation for the design of a magnetic levitation ventricular-assist nutation pump.

However, it was unclear whether the magnetic levitation of the spherical bearing could be stable. Moreover, because the pump is driven by magnetic coupling from the outside, the radial size of the pump is increased. For the next step, we are developing an electromagnetically driven model in which magnets in the disk are driven by coils. In this model, a method to monitor the levitated clearance with an eddy current displacement sensor will be tested to study the magnetic levitation stability of the pump. Additionally, to develop a practical blood pump, further improvements, especially the efficiency, motor control, durability, etc., are the next subjects of future research.

REFERENCES

[1] K. Espeed and H. D. John, "Heart transplantation," *Surgery*, vol. 35, no. 7, pp. 360–364, 2017.
[2] E. Okamoto, Y. Ishida, T. Yano, and Y. Mitamura, "Passive magnetic bearing in the 3rd generation miniature axial flow pump-the valvo pump 2," *J. Artif. Organs*, vol. 18, no. 2, pp. 181–184, Jun. 2015.
[3] S. J. Pettit, L. M. Shapiro, C. Lewis, J. K. Parameshwar, and S. S. L. Tsui, "Percutaneous withdrawal of HeartWare HVAD left ventricular assist device support," *J. Heart Lung Transplantation*, vol. 34, no. 7, pp. 990–992, Jul. 2015.
[4] G. Heatley, P. Sood, D. Goldstein, N. Uriel, J. Cleveland, D. Middlebrook, and M. R. Mehra, "Clinical trial design and rationale of the Multicenter Study of MagLev Technology in Patients Undergoing Mechanical Circulatory Support Therapy With HeartMate 3 (MOMENTUM 3) investigational device exemption clinical study protocol," *J. Heart Lung Transplantation*, vol. 35, no. 4, pp. 528–536, Apr. 2016.

[5] Y. Sawa, "Current status of third-generation implantable left ventricular assist devices in Japan, Duraheart and HeartWare," *Surg. Today*, vol. 45, no. 6, pp. 672–681, Jun. 2015.
[6] A. Tschirkov, D. Nikolov, and V. Papantchev, "New technique for implantation of the inflow canula of Berlin Heart INCOR system," *Eur. J. Cardio-Thoracic Surg.*, vol. 30, no. 4, pp. 678–679, Oct. 2006.
[7] M. Koochaki and H. Niroomand-Oscuii, "A new design and computational fluid dynamics study of an implantable axial blood pump," *Australas. Phys. Eng. Sci. Med.*, vol. 36, no. 4, pp. 417–422, Dec. 2013.
[8] Y. Abe, T. Isoyama, I. Saito, M. Ono, S. Mochizuki, H. Nakagawa, N. Taniguchi, N. Mitsumune, A. Sugino, M. Mitsui, K. Takiura, T. Ono, A. Kouno, T. Chinzei, S. Takamoto, and K. Imachi, "Development of mechanical circulatory support devices at the University of Tokyo," *J. Artif. Organs*, vol. 10, no. 2, pp. 60–70, Jun. 2007.
[9] Y. Abe, T. Isoyama, I. Saito, Y. Inoue, K. Ishii, H. Nakagawa, T. Ono, M. Ono, K. Imachi, and W. Shi, "Results of animal experiments with the fourth model of the undulation pump total artificial heart," *J. Artif. Organs*, vol. 35, no. 8, pp. 781–790, Aug. 2011.
[10] J. He, L. Yao, H. Shen, and R. Zheng, "Feasibility analysis and design of a novel ventricular assist miniscule nutation pump," in *Proc. 25th Design Conf. Innov. Product Creation (CIRP)*, Haifa, Israel, Oct. 2015, pp. 273–278.
[11] F. X. Lin, "The simulation analysis and experiment for the fluid flow characteristics of the novel ventricular assist miniscule nutation pump," M.S. thesis, Dept. Mech. Eng. Auto., Fuzhou Univ., Fuzhou, China, 2017.
[12] M. Stoiber, C. Grasl, S. Pirker, F. Raderer, R. Schistek, L. Huber, P. Gittler, and H. Schima, "A passive magnetically and hydrodynamically suspended rotary blood pump," *Artif. Organs*, vol. 33, no. 3, pp. 250–257, Mar. 2009.
[13] T. Masuzawa, "Magnetically suspended motor system applied to artificial hearts and blood pumps," *Proc. Inst. Mech. Eng. I, J. Syst. Control Eng.*, vol. 231, no. 5, pp. 330–338, Apr. 2016.
[14] T. Masuzawa, S. Ezoe, T. Kato, and Y. Okada, "Magnetically suspended centrifugal blood pump with an axially levitated motor," *Artif. Organs*, vol. 27, no. 7, pp. 631–638, Jul. 2003.
[15] P. E. Allaire, R. Flack, D. B. Olsen, J. W. Long, A. B. Kumar, P. S. Khanwilkar, J. Decker, M. Baloh, and G. B. Bearnson, "Implantable centrifugal pump with hybrid magnetic bearings," U.S. Patents 2014 0 314 597, Jul. 1, 2014.
[16] A. Hamler, V. Gorican, B. Štumberger, M. Jesenik, and M. Trlep, "Passive magnetic bearing," *J. Magn. Magn. Mater.*, vol. 272, pp. 2379–2380, May 2004.
[17] F. K. Wan, P. Zeng, W. M, Ru, H. Y. Yuan, and K. X Qian, "Permanent Maglev impeller blood pump and analysis of its rotator suspension," *Beijing J. Biomed. Eng.*, vol. 24, no. 3, pp. 199–203, 2005.
[18] K.-X. Qian, "Methods of stabilizing a permanent Maglev rotator in heart pumps and other rotary machines," *Global J. Cardiovasc. Cerebrovasc. Dis.*, vol. 2, no. 3, pp. 6–13, 2014.
[19] R. Ravaud, G. Lemarquand, V. Lemarquand, and C. Depollier, "Analytical calculation of the magnetic field created by permanent-magnet rings," *IEEE Trans. Magn.*, vol. 44, no. 8, pp. 1982–1989, Aug. 2008.
[20] R. Ravaud, G. Lemarquand, V. Lemarquand, and C. Depollier, "Magnetic field produced by a tile permanent magnet whose polarization is both uniform and tangential," *Prog. Electromagn. Res. B*, vol. 13, no. 13, pp. 1–20, Mar. 2009.
[21] K. D. Bachovchin, J. F. Hoburg, and R. F. Post, "Magnetic fields and forces in permanent magnet levitated bearings," *IEEE Trans. Magn.*, vol. 48, no. 7, pp. 2112–2120, Jul. 2012.
[22] X. Sun, L. Chen, Z. Yang, and H. Zhu, "Speed-sensorless vector control of a bearingless induction motor with artificial neural network inverse speed observer," *IEEE/ASME Trans. Mechatronics*, vol. 18, no. 4, pp. 1357–1366, Aug. 2013.
[23] X. Sun, B. Su, S. Wang, Z. Yang, G. Lei, J. Zhu, and Y. Guo, "Performance analysis of suspension force and torque in an IBPMSM with V-shaped PMs for flywheel batteries," *IEEE Trans. Magn.*, vol. 54, no. 11, Nov. 2018, Art. no. 8105504.
[24] X. Sun, Z. Jin, S. Wang, Z. Yang, K. Li, Y. Fan, and L. Chen, "Performance improvement of torque and suspension force for a novel five-phase BFSPM machine for flywheel energy storage systems," *IEEE Trans. Appl. Supercond.*, vol. 29, no. 2, Mar. 2019, Art. no. 0601505.
[25] X. Sun, Z. Shi, L. Chen, and Z. Yang, "Internal model control for a bearingless permanent magnet synchronous motor based on inverse system method," *IEEE Trans. Energy Convers.*, vol. 31, no. 4, pp. 1539–1548, Dec. 2016.
[26] D. Xia, "A bionic artificial heart blood pump driven by permanent magnet located outside human body," *IEEE Trans. Appl. Supercond.*, vol. 22, no. 3, Jun. 2012, Art. no. 4401304.
[27] Y. Oner and S. Kesler, "3D magnetic analysis of permanent magnets in spherical configuration," *J. Elect. Eng. Technol.*, vol. 11, no. 1, pp. 709–715, Jan. 2015.
[28] Q.-C. Tan, F.-S. Zheng, and J.-G. Li, "Magnetic force transmission of a reciprocating motion," *J. Bionic Eng.*, vol. 5, no. 2, pp. 143–147, Jun. 2008.
[29] Q.-C. Tan, W. Li, and B. Liu, "Investigations on a permanent magnetic–hydrodynamic hybrid journal bearing," *Tribol. Int.*, vol. 35, no. 7, pp. 443–448, Jul. 2002.
[30] Q.-C. Tan, D. Xin, W. Li, and H. Meng, "Study on transmitting torque and synchronism of magnet couplings," *Proc. Inst. Mech. Eng. C, J. Mech. Eng. Sci.*, vol. 206, no. 6, pp. 381–384, Nov. 1992.
[31] J.-G. Li, Q.-C. Tan, and Y.-C. Pei, "Influence of non-coaxial alignment on interaction forces for the contactless magnetic driver of a reciprocating motion," *Int. J. Appl. Electrom. Mech.*, vol. 49, no. 2, pp. 169–177, Oct. 2015.
[32] J. D. Jackson, "Classical electrodynamics," *Phys. Today*, vol. 15, no. 11, p. 11, 1975.
[33] T. I. Khan, Z. H. Sheh, I. Lazoglu, and O. Yalcin, "Development of a novel shrouded impeller pediatric blood pump," *J. Artif. Organs*, vol. 21, no. 2, pp. 142–149, Jun. 2018.
[34] *Standard Practice for Assessment of Hemolysis in Continuous Flow Blood Pumps*, Standard ASTM F1841-97, American Society for Testing and Materials, New York, NY, USA, 2013.
[35] A. L. Throckmorton, J. Y. Kapadia, S. G. Chopski, S. S. Bhavsar, W. B. Moskowitz, S. D. Gullquist, J. J. Gangemi, C. M. Haggerty, and A. P. Yoganathan, "Numerical, hydraulic, and hemolytic evaluation of an intravascular axial flow blood pump to mechanically support Fontan patients," *Ann. Biomed. Eng.*, vol. 39, no. 1, pp. 324–336, Jan. 2011.
[36] J.-H. Yen, S.-F. Chen, M.-K. Chern, and P.-C. Lu, "The effect of turbulent viscous shear stress on red blood cell hemolysis," *J. Artif. Organs*, vol. 17, no. 2, pp. 178–185, Jun. 2014.
[37] S. Lee, Y. Cho, S. Kang, N. Hur, and Y. Kim, "Evaluation of an extended viscoelastic model to predict hemolysis in cannulas and blood pumps," *J. Mech. Sci. Technol.*, vol. 33, no. 5, pp. 2181–2188, May 2019.
[38] R. Paul, J. Apel, S. Klaus, F. Schügner, P. Schwindke, and H. Reul, "Shear stress related blood damage in laminar couette flow," *Artif. Organs*, vol. 27, no. 6, pp. 517–529, Jun. 2003.
[39] H. Niimi and M. Sugihara, "Cyclic loading on the red cell membrane in a shear flow: A possible cause of hemolysis," *J. Biomech. Eng. Trans.*, vol. 107, no. 2, pp. 91–95, Jun. 1985.

GANG CHEN received the M.S. degree in vehicle engineering from Chang'an University, Xi'an, China, in 2012. He is currently pursuing the Ph.D. degree in mechanical design and theory with the School of Mechanical Engineering and Automation, Fuzhou University, Fuzhou, China. He is also a Lecturer with Fujian Sanming University. His current research interests include magnetic transmission, modern design method, and precision manufacturing. He is a member of the Chinese Mechanical Engineering Society.

LIGANG YAO received the Ph.D. degree in mechanical engineering from the Harbin Institute of Technology, China, in 1996.

He is currently the Director of the Gear Laboratory, Fuzhou University, where he is also a Professor with the School of Mechanical Engineering and Automation. He has published more than 70 international journal articles. His research interests include robot mechanism and mechanical transmission, rehabilitation robot, modern design method, complex surface modeling, and precision manufacturing. He is also a member of the ASME and a Senior Member of the Chinese Mechanical Engineering Society. He has served as a Reviewer of related journals for years.

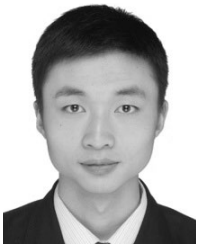

RONGYE ZHENG received the B.S., M.S., and Ph.D. degrees in fluid machinery and engineering from Xi'an Jiaotong University, China, in 2004, 2008, and 2014, respectively. He is currently a Lecturer with the School of Mechanical Engineering and Automation. His current research interests include fluid machinery, computational models and algorithms for single-phase and multiphase flows, and optimum design method.

LONG ZHANG received the M.S. degree in mechanical engineering from Fuzhou University, Fuzhou, China, in 2019. He is currently an Assistant Engineer with Fujian Hongfa Group Company, Ltd. His current research interests include fluid machinery, finite element analysis, and digital design.

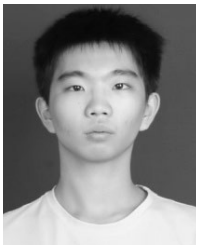

JIAXIN DING received the B.E. degree in vehicle engineering from the Fujian University of Technology, Fuzhou, China, in 2017. He is currently pursuing the master's degree in mechanical engineering with the School of Mechanical Engineering and Automation, Fuzhou University, Fuzhou. His current research interests include nutation drive, magnetic gear reducer, and dynamic analysis.